Two time scale approach

In this chapter, a joint impedance controller is designed by building a joint controller upon the tendon force controller. Two different designs are presented: the first one is using the singular perturbation approach and the second one is using the cascaded approach.

The singular perturbation approach relies upon the time scale difference between the tendon force controller and the link side dynamics. This assumption is similar to the one made when considering the motors as torque sources while commanding currents or voltages. In the Awiwi Hand the stiffness is modified by the internal pretension, thus modifying the time scale differences. Moreover, the assumption is only partially valid in the case of fingers since the links have a low inertia and the motors, together with the gear boxes, have larger inertias. It can be expected, and it is experimentally verified that the validity of the singular perturbation assumption depends on the mechanical stiffness. In the first case, the outer loop is considered as constant for the inner loop. The inner loop error is neglected arguing that, because of its speed, the inner loop is stabilized before the outer loop is *disturbed*. Despites its limitations it remains a good technique to approach the problem thanks to its intuitive structure.

In the second case, namely the cascaded approach, the system is brought into a cascaded form, that is, a triangular system. The stability is obtained by explicitly considering the inner loop tracking error as a forcing term for the outer loop. However, the analysis is more complex than in the singular perturbation case.

This chapter applies both methods to the case of a flexible joint, the difference being essentially visible in the stability proofs. In the first section the dynamic model is transformed into a cascaded form. Then, the tendon force controller designed in the previous chapter is augmented with some feedforward terms and their influence is experimentally verified. Next, the equations of a joint impedance controller are established by considering that a torque source is available at the joint. The next sections are establishing stability in the case of the singular perturbation approach and the cascaded approach. Finally, experimental results are presented. They highlight that increasing the internal pretension reduces the validity the singular perturbation approach.

11.1 Model

Under the assumption that the tendon force controller and the link impedance controller are working in two *independent* frequency domains the dynamic

equations of a finger can be written as

$$\boldsymbol{B}\ddot{\boldsymbol{\theta}} = -\boldsymbol{E}^T \boldsymbol{f}_{\mathrm{t}}(\boldsymbol{\theta} - \boldsymbol{q}_0) + \boldsymbol{\tau}_{\mathrm{m}} + \boldsymbol{b}(\boldsymbol{\theta}, \dot{\boldsymbol{\theta}}) \ , \tag{11.1}$$

where the link position $\boldsymbol{q}_0$ is considered to be constant w. r. t. the scale of the motor dynamics. When considering m tendons, $\boldsymbol{B} \in \mathbb{R}^{m \times m}$ is a diagonal motor inertia matrix, $\boldsymbol{\theta} \in \mathbb{R}^m$ is the vector of the motor positions, $\boldsymbol{E} \in \mathbb{R}^{m \times m}$ is a diagonal matrix of the pulley radius, $\boldsymbol{f}_{\mathrm{t}} \in \mathbb{R}^m$ is the vector of the tendon forces. The electromagnetic torque is denoted $\boldsymbol{\tau}_{\mathrm{m}} \in \mathbb{R}^m$. Following the same approach, the link side equations are modified to integrate the fact that the tendon forces are the input variables.

$$\boldsymbol{M}(\boldsymbol{q})\ddot{\boldsymbol{q}} + \boldsymbol{C}(\boldsymbol{q}, \dot{\boldsymbol{q}})\dot{\boldsymbol{q}} + \boldsymbol{g}(\boldsymbol{q}) + \boldsymbol{b}(\boldsymbol{q}, \dot{\boldsymbol{q}}) = \boldsymbol{P}^T \boldsymbol{f}_{\mathrm{t}} + \boldsymbol{\tau}_{\mathrm{ext}} \ . \tag{11.2}$$

When considering n links, $\boldsymbol{M}(\boldsymbol{q}) \in \mathbb{R}^{n \times n}$ is the link inertia matrix, $\boldsymbol{q} \in \mathbb{R}^n$ is the vector of the joint positions, $\boldsymbol{C}(\boldsymbol{q}, \dot{\boldsymbol{q}})\dot{\boldsymbol{q}} \in \mathbb{R}^n$ is the vector of the Coriolis and centrifugal terms, $\boldsymbol{P} \in \mathbb{R}^{n \times m}$ is the coupling matrix, $\boldsymbol{f}_{\mathrm{t}} \in \mathbb{R}^m$ is the vector of the tendon forces. The external torques and the vector of joint frictional torques are represented by $\boldsymbol{\tau}_{\mathrm{ext}} \in \mathbb{R}^n$ and $\boldsymbol{b}(\boldsymbol{q}, \dot{\boldsymbol{q}}) \in \mathbb{R}^n$.

11.2 Tendon Controller Design

The control of the tendon force is realized by a PD controller with a feedforward term for the expected torque generated by the tendon force. A friction compensation term, $\hat{\boldsymbol{b}}(\boldsymbol{\theta}, \dot{\boldsymbol{\theta}})$, is added to further improve the transient response. It is structurally similar to the tendon controller with gain scheduling but the gains are constant in order to facilitate the analysis.

$$\boldsymbol{\tau}_{\mathrm{m}} = \boldsymbol{E}^T \left(\boldsymbol{f}_{\mathrm{t}} + \boldsymbol{K}_{\mathrm{p}}(\boldsymbol{\theta}_{\mathrm{des}} - \boldsymbol{\theta}) - \boldsymbol{K}_{\mathrm{d}}\dot{\boldsymbol{\theta}} + \hat{\boldsymbol{b}}(\boldsymbol{\theta}, \dot{\boldsymbol{\theta}}) \right) \ , \tag{11.3}$$

where $\boldsymbol{\theta}_{\mathrm{des}} \in \mathbb{R}^m$ is the motor position vector that would generate the desired force vector. The friction model identified in the modeling chapter is represented by $\hat{\boldsymbol{b}}(\boldsymbol{\theta}, \dot{\boldsymbol{\theta}})$. The force tracking and motor damping gain matrices are diagonal and positive definite. They are denoted $\boldsymbol{K}_{\mathrm{p}} \in \mathbb{R}^{m \times m}$ and $\boldsymbol{K}_{\mathrm{d}} \in \mathbb{R}^{m \times m}$. Figure 11.1a shows the simulation results obtained with and without a feedforward force component. Fig. 11.1b shows the influence of the friction compensation on the rise time of the force step response. The improvements in settling time are limited by the saturation of the control and the control delay ($333\mu s$).

11.3 Link Controller Design

The link side dynamics are designed as a regular impedance controller [78]. The link side torque input is,

$$\boldsymbol{\tau}_{\mathrm{des}} = \boldsymbol{M}(\hat{\boldsymbol{q}})\ddot{\boldsymbol{q}}_{\mathrm{des}} + \boldsymbol{C}(\hat{\boldsymbol{q}}, \dot{\hat{\boldsymbol{q}}})\dot{\boldsymbol{q}}_{\mathrm{des}} + \boldsymbol{K}_{\mathrm{p,imp}}(\boldsymbol{q}_{\mathrm{des}} - \hat{\boldsymbol{q}}) + \boldsymbol{K}_{\mathrm{d,imp}}(\dot{\boldsymbol{q}}_{\mathrm{des}} - \dot{\hat{\boldsymbol{q}}}) + \hat{\boldsymbol{b}}(\hat{\boldsymbol{q}}, \dot{\hat{\boldsymbol{q}}}) + \boldsymbol{g}(\hat{\boldsymbol{q}}) \ , \tag{11.4}$$

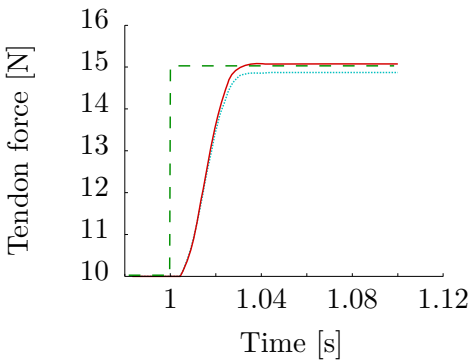

(a) Tendon force step response, without desired force feedforward and with force feedforward

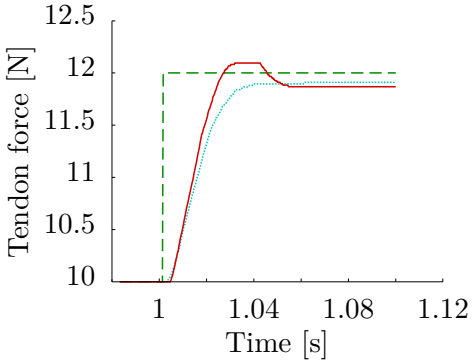

(b) Tendon force step response, with and without friction compensation

Figure 11.1: Tendon force controller experiments. The green/dashed line depicts the desired tendon force. The measured tendon force is represented in red/solid (resp. in light blue/dotted) for the case with feedforward term (resp. without).

where $\hat{.}$ denotes an estimated quantity, obtained by a linear observer or a filtering process (e. g. using a low pass or a Kalman filter). The joint position vector (resp. the desired joint position vector) is denoted $\boldsymbol{q} \in \mathbb{R}^n$ (resp. $\boldsymbol{q}_{\text{des}} \in \mathbb{R}^n$). The terms $\boldsymbol{M}(\boldsymbol{q}) \in \mathbb{R}^{n \times n}$, $\boldsymbol{C}(\boldsymbol{q}, \dot{\boldsymbol{q}}) \in \mathbb{R}^{n \times n}$ and $\boldsymbol{g}(\boldsymbol{q}) \in \mathbb{R}^n$ are the link inertia matrix, the vector of the Coriolis torques and the vector of gravity torques. The vector of frictional torques identified in the modeling section is represented by $\boldsymbol{b}(\boldsymbol{\theta}, \dot{\boldsymbol{\theta}})$. The impedance and damping matrices (positive definite) are denoted $\boldsymbol{K}_{\text{p,imp}} \in \mathbb{R}^{m \times m}$ and $\boldsymbol{K}_{\text{d,imp}} \in \mathbb{R}^{m \times m}$. The term $\boldsymbol{M}(\hat{\boldsymbol{q}})\ddot{\boldsymbol{q}}_{\text{des}}$ is traditionally used to improve the tracking performance but has only little influence in the case of fingers. The desired tendon forces that are required to generate the joint torque for the impedance controller are obtained with the help of the coupling matrix pseudo-inverse.

11.4 Stability Conditions: The singular perturbation case

In this section, the stability conditions are derived for the link controller and the tendon controller. Finally the stability of the closed-loop system is concluded, under the singular perturbation hypothesis.

Tendon force controller

In order to establish the stability conditions, the Lyapunov method is used. All tendons are assumed to be independent and therefore all matrices are simply diagonal. For the tendon force controller, the Lyapunov candidate

function is defined as

$$V(\boldsymbol{\theta}) = \frac{1}{2}\dot{\boldsymbol{\theta}}^T \boldsymbol{B}\dot{\boldsymbol{\theta}} + V_{\mathrm{k}}(\boldsymbol{\theta}) - V_{\mathrm{k}}(\boldsymbol{\theta}_{\mathrm{des}}) + \left.\frac{\partial V_{\mathrm{k}}}{\partial \boldsymbol{\theta}}\right|_{\boldsymbol{\theta}_{\mathrm{des}}} (\boldsymbol{\theta}_{\mathrm{des}} - \boldsymbol{\theta})^T + \frac{1}{2}(\boldsymbol{\theta} - \boldsymbol{\theta}_{\mathrm{des}})^T \boldsymbol{K}_{\mathrm{p}}(\boldsymbol{\theta} - \boldsymbol{\theta}_{\mathrm{des}}) \,, \tag{11.5}$$

where $\boldsymbol{\theta}_{\mathrm{des}} = \phi^{-1}(\boldsymbol{f}_{\mathrm{t,des}})$ is the motor position that would result in the desired tendon force. The storage function of the spring is denoted $V_{\mathrm{k}}(\theta) = \int_0^{\theta} f(x)dx$. The Lyapunov function is composed of the kinetic energy, the spring elastic energy, and the expected energy at the equilibrium point. The time derivative is

$$\dot{V}(\boldsymbol{\theta}) = \dot{\boldsymbol{\theta}}^T \boldsymbol{B}\ddot{\boldsymbol{\theta}} + \dot{\boldsymbol{\theta}}^T \frac{\partial V_{\mathrm{k}}}{\partial \boldsymbol{\theta}} - \left.\frac{\partial V_{\mathrm{k}}}{\partial \boldsymbol{\theta}}\right|_{\boldsymbol{\theta}_{\mathrm{des}}} \dot{\boldsymbol{\theta}}^T - \dot{\boldsymbol{\theta}}^T \boldsymbol{K}_{\mathrm{p}}(\boldsymbol{\theta}_{\mathrm{des}} - \boldsymbol{\theta}) \,. \tag{11.6}$$

Replacing the expression of V_{k}, as well as the controller equations yields

$$\dot{V}(\boldsymbol{\theta}) = \dot{\boldsymbol{\theta}}^T (\boldsymbol{f}_{\mathrm{t,des}} - \boldsymbol{K}_{\mathrm{p}}(\boldsymbol{\theta}_{\mathrm{des}} - \boldsymbol{\theta}) - \boldsymbol{K}_{\mathrm{d}}\dot{\boldsymbol{\theta}} + \hat{\boldsymbol{b}} - \boldsymbol{b} + \boldsymbol{f}_{\mathrm{t}}) + \dot{\boldsymbol{\theta}}^T \boldsymbol{f}_{\mathrm{t}} - \dot{\boldsymbol{\theta}}^T \boldsymbol{\phi}(\boldsymbol{\theta}_{\mathrm{des}}) - \dot{\boldsymbol{\theta}}^T \boldsymbol{K}_{\mathrm{p}}(\boldsymbol{\theta}_{\mathrm{des}} - \boldsymbol{\theta}) \,. \tag{11.7}$$

Since $\boldsymbol{f}_{\mathrm{des}} = \boldsymbol{\phi}(\boldsymbol{\theta}_{\mathrm{des}})$:

$$\dot{V}(\boldsymbol{\theta}) = -\dot{\boldsymbol{\theta}}^T (\boldsymbol{K}_{\mathrm{d}}\dot{\boldsymbol{\theta}} + \hat{\boldsymbol{b}} - \boldsymbol{b}) \,. \tag{11.8}$$

As long as the viscous friction is not overestimated or at least less than the damping injected by the controller, the term $(\boldsymbol{K}_{\mathrm{d}}\dot{\boldsymbol{\theta}} + \hat{\boldsymbol{b}} - \boldsymbol{b})$ is positive, thereby ensuring that the derivative of the Lyapunov function is negative semi-definite. Finally, the global asymptotic stability is obtained by invoking the LaSalle theorem.

Positive definiteness of V The terms $\dot{\boldsymbol{\theta}}^T \boldsymbol{B}\dot{\boldsymbol{\theta}}$ and $(\boldsymbol{\theta} - \boldsymbol{\theta}_{\mathrm{des}})^T \boldsymbol{K}_p(\boldsymbol{\theta} - \boldsymbol{\theta}_{\mathrm{des}})$ are positive definite due to the fact that $\boldsymbol{B} > 0$ and $\boldsymbol{K}_{\mathrm{p}} > 0$. It remains to prove that $\Gamma(\boldsymbol{\theta}) = V_{\mathrm{k}}(\boldsymbol{\theta}) - V_{\mathrm{k}}(\boldsymbol{\theta}_{\mathrm{des}}) + \frac{\partial V_{\mathrm{k}}}{\partial \boldsymbol{\theta}}|_{\boldsymbol{\theta}_{\mathrm{des}}}(\boldsymbol{\theta}_{\mathrm{des}} - \boldsymbol{\theta})^T$ is positive definite. Trivially, $\Gamma(\boldsymbol{\theta}_{\mathrm{des}}) = \boldsymbol{0}$. Γ has an extremum in $\boldsymbol{\theta}_{\mathrm{des}}$ since $\frac{\partial \Gamma}{\partial \boldsymbol{\theta}}(\boldsymbol{\theta}_{\mathrm{des}}) = \frac{\partial V_{\mathrm{k}}}{\partial \boldsymbol{\theta}}(\boldsymbol{\theta}_{\mathrm{des}}) - \frac{\partial V_{\mathrm{k}}}{\partial \boldsymbol{\theta}}|_{\boldsymbol{\theta}_{\mathrm{des}}} = \boldsymbol{0}$. It is a minimum because $\frac{\partial^2 \Gamma}{\partial \boldsymbol{\theta}^2} = \frac{\partial \phi(\boldsymbol{\theta})}{\partial \boldsymbol{\theta}} > 0$ because $\boldsymbol{f}_{\mathrm{t}} = \boldsymbol{\phi}(\boldsymbol{\theta})$ is strictly increasing, which completes the proof.

Link side controller

The equations for the link side dynamics and the link side controller are

$$\boldsymbol{M}(\boldsymbol{q})\ddot{\boldsymbol{q}} + \boldsymbol{C}(\dot{\boldsymbol{q}}, \boldsymbol{q})\dot{\boldsymbol{q}} + \boldsymbol{g}(\boldsymbol{q}) = \boldsymbol{\tau}_{\mathrm{ext}} + \boldsymbol{\tau} \tag{11.9}$$

and

$$\boldsymbol{\tau} = -\boldsymbol{K}_{\mathrm{p,imp}}(\boldsymbol{q} - \boldsymbol{q}_{\mathrm{des}}) - \boldsymbol{K}_{\mathrm{d,imp}}(\boldsymbol{q} - \boldsymbol{q}_{\mathrm{des}}) + \boldsymbol{g}(\boldsymbol{q}) + \boldsymbol{C}(\dot{\boldsymbol{q}}, \boldsymbol{q})\dot{\boldsymbol{q}}_{\mathrm{des}} + \boldsymbol{M}(\boldsymbol{q})\ddot{\boldsymbol{q}}_{\mathrm{des}}. \tag{11.10}$$

The regulation problem is used to prove stability, that is, $\boldsymbol{q}_{\mathrm{des}} = \dot{\boldsymbol{q}}_{\mathrm{des}} = \ddot{\boldsymbol{q}}_{\mathrm{des}} = \boldsymbol{0}$. The two following paragraphs present two alternative proofs.

Lyapunov Approach Consider the Lyapunov function

$$V(\boldsymbol{q}, \dot{\boldsymbol{q}}) = \frac{1}{2}\dot{\boldsymbol{q}}^T \boldsymbol{M}(\boldsymbol{q})\dot{\boldsymbol{q}} + \frac{1}{2}\boldsymbol{q}^T \boldsymbol{K}_{\mathrm{p,imp}}\boldsymbol{q} \ . \tag{11.11}$$

Its derivative along the solutions is

$$\dot{V}(\boldsymbol{q}, \dot{\boldsymbol{q}}) = \dot{\boldsymbol{q}}^T \boldsymbol{M}(\boldsymbol{q})\ddot{\boldsymbol{q}} + \frac{1}{2}\dot{\boldsymbol{q}}^T \dot{\boldsymbol{M}}(\boldsymbol{q})\dot{\boldsymbol{q}} + \dot{\boldsymbol{q}}^T \boldsymbol{K}_{\mathrm{p,imp}}\boldsymbol{q} \ . \tag{11.12}$$

Replacing the controller equation in free environment leads to

$$\dot{V}(\boldsymbol{q}, \dot{\boldsymbol{q}}) = \dot{\boldsymbol{q}}^T(\boldsymbol{\tau} - \boldsymbol{C}(\dot{\boldsymbol{q}}, \boldsymbol{q}) + \boldsymbol{g}(\boldsymbol{q})) + \frac{1}{2}\dot{\boldsymbol{q}}^T \dot{\boldsymbol{M}}(\boldsymbol{q})\dot{\boldsymbol{q}} + \dot{\boldsymbol{q}}^T \boldsymbol{K}_{\mathrm{p,imp}}\boldsymbol{q} \ , \tag{11.13}$$

which is further simplified to

$$\dot{V}(\boldsymbol{q}, \dot{\boldsymbol{q}}) = -\dot{\boldsymbol{q}}^T \boldsymbol{K}_{\mathrm{d,imp}}\dot{\boldsymbol{q}} \ . \tag{11.14}$$

Since $\boldsymbol{K}_{\mathrm{d,imp}}$ is positive definite, the Lyapunov derivative is negative semi-definite. The global asymptotic stability is concluded by invoking the LaSalle theorem.

Alternative proof By design the closed-loop dynamics of the error $\boldsymbol{e} = \boldsymbol{q}_{\mathrm{des}} - \boldsymbol{q}$ is

$$\boldsymbol{M}(\boldsymbol{q})\ddot{\boldsymbol{e}} + \boldsymbol{K}_{\mathrm{d,imp}}\dot{\boldsymbol{e}} + \boldsymbol{K}_{\mathrm{p,imp}}\boldsymbol{e} = 0. \tag{11.15}$$

The stability is ensured by the choice of the stiffness and the damping matrices (which ought to be positive definite).

11.5 Stability Conditions : The cascaded case

The previous section neglected the influence of the force controller error and established the closed-loop stability under the singular perturbation hypothesis. It is possible to explicitly take into account the tendon force error if the system is considered as a cascaded system. However, because the systems must depend on the same set of variables, the linearizing tendon force controller is used instead of the motor position controller. As a result, a differential system of equations in the variable θ is considered. The initial system, under the action of the controller is given by:

$$\begin{aligned} \boldsymbol{B}_{\mathrm{f}}\ddot{\boldsymbol{e}}_{\mathrm{f}} + \boldsymbol{K}_{\mathrm{p}}\dot{\boldsymbol{e}}_{\mathrm{f}} + \boldsymbol{K}_{\mathrm{p}}\boldsymbol{e}_{\mathrm{f}} = 0 \\ \boldsymbol{M}\ddot{\boldsymbol{q}} + \boldsymbol{K}_{\mathrm{d,imp}}(\dot{\boldsymbol{q}} - \dot{\boldsymbol{q}}_{\mathrm{des}}) + \boldsymbol{K}_{\mathrm{p,imp}}(\boldsymbol{q} - \boldsymbol{q}_{\mathrm{des}}) = \boldsymbol{P}^T\boldsymbol{e}_{\mathrm{f}} \ . \end{aligned} \tag{11.16}$$

where $\boldsymbol{e}_{\mathrm{f}} = \boldsymbol{f}_{\mathrm{t,des}} - \boldsymbol{f}_{\mathrm{t}}$ is the tendon force error. To establish stability, the two decoupled system must be asymptotically stable. Moreover, the coupled system must be proved to be stable. Then, the global system is asymptotically stable. The construction of the proof is inspired by Ott [130]. The first

conditions are trivially obtained given that the gain matrices are positive definite. Even exponential stability is possible. The second condition, however, is more subtle. The solution consists in building a quadratic Lyapunov function for which it is possible to show that there always exists a choice of gains that ensures stability. A candidate Lyapunov function is given by

$$V(\boldsymbol{q}, \dot{\boldsymbol{q}}, \boldsymbol{e}) = \frac{1}{2}\dot{\boldsymbol{q}}^T \boldsymbol{M}\dot{\boldsymbol{q}} + \frac{1}{2}\boldsymbol{q}^T \boldsymbol{K}_{\mathrm{p,imp}}\boldsymbol{q} + \boldsymbol{e}^T \boldsymbol{G}\boldsymbol{e} \ , \tag{11.17}$$

where all matrices are positive definite, thus being a quadratic Lyapunov function. The derivative of the candidate along the solution of the system is

$$\begin{aligned}\dot{V}(\boldsymbol{q}, \dot{\boldsymbol{q}}, \boldsymbol{e}) = \dot{\boldsymbol{q}}^T(-\boldsymbol{K}_{\mathrm{d,imp}}(\dot{\boldsymbol{q}} - \boldsymbol{q}_{\mathrm{des}}) - \boldsymbol{K}_{\mathrm{p,imp}}(\boldsymbol{q} - \boldsymbol{q}_{\mathrm{des}}) + \boldsymbol{P}^T\boldsymbol{e}_{\mathrm{f}}) \\ +\boldsymbol{q}^T\boldsymbol{K}_{\mathrm{p,imp}}\dot{\boldsymbol{q}} + \tfrac{1}{2}\dot{\boldsymbol{e}}^T\boldsymbol{G}\boldsymbol{e} + \tfrac{1}{2}\boldsymbol{e}^T\boldsymbol{G}\dot{\boldsymbol{e}}\end{aligned} \ . \tag{11.18}$$

In the regulation case, it simplifies to

$$\dot{V}(\boldsymbol{q}, \dot{\boldsymbol{q}}, \boldsymbol{e}) = -\dot{\boldsymbol{q}}^T\boldsymbol{K}_{\mathrm{d,imp}}\dot{\boldsymbol{q}} - \dot{\boldsymbol{q}}^T\boldsymbol{P}^T\boldsymbol{e}_{\mathrm{f}} + \dot{\boldsymbol{e}}^T\boldsymbol{G}\boldsymbol{e} \ , \tag{11.19}$$

which can be rewritten in the following matrix form by defining a state vector $w = [\dot{\boldsymbol{q}}, \boldsymbol{e}, \dot{\boldsymbol{e}}]$.

$$\dot{V}(\boldsymbol{w}) = -\boldsymbol{w}^T\boldsymbol{W}\boldsymbol{w}. \tag{11.20}$$

The matrix $\boldsymbol{W}$ is given by

$$\boldsymbol{W} = \begin{bmatrix} \boldsymbol{K}_{\mathrm{d,imp}} & \boldsymbol{P}^T/2 \\ \boldsymbol{P}/2 & -\boldsymbol{G} \end{bmatrix} \ . \tag{11.21}$$

According to Schur's Lemma the matrix is positive definite if $\boldsymbol{K}_{\mathrm{d,imp}} > \boldsymbol{0}$ and $\boldsymbol{K}_{\mathrm{d,imp}} - \frac{1}{4}\boldsymbol{P}^T\boldsymbol{G}^{-1}\boldsymbol{P} > \boldsymbol{0}$. The first condition is trivially fulfilled while the second one can always be satisfied by a good choice of a positive definite $\boldsymbol{G}$. Since $\boldsymbol{G}$ can be selected freely as being one solution of the Riccati equation, the system is globally stable. Together with the exponential stability of the subsystems, the cascaded system is globally asymptotically stable.

11.6 Experimental Results

The performance of the singular perturbation and the cascaded approaches would optimally be analyzed in three separated setups: a single tendon motor unit with motor torque input, a finger with a *direct* joint torque input and the combination of a tendon force controller and the joint torque impedance controller. However, it is not possible to create a direct joint torque controller, since the hardware can not be adapted for it. Nonetheless, previous experiments with the DLR Hand II, where the motors are directly located in the joints, confirmed the validity of the design. The experimental results of the tendon controller have been reported in the previous chapter.

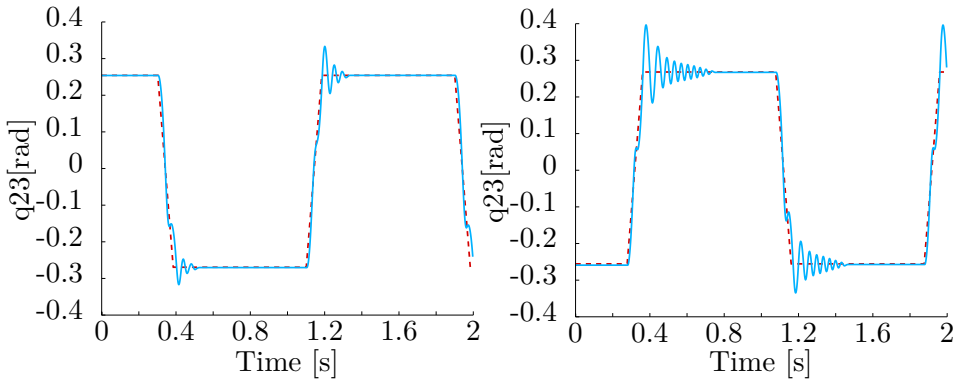

(a) Low impedance stiffness

(b) High impedance stiffness

Figure 11.2: Experiment: step response for two impedance controller stiffness

Therefore, this chapter reports only the controller results corresponding to the complete system.

A simple experiment allows to verify the basic functionality of the link side controller. A desired position change of the link is commanded with two different impedance stiffness. Because the low damping of the impedance is left unchanged, as well as the other controller parameters, the oscillations should be increasing. In Figure 11.2, the desired link position is depicted in dashed/red and the measured link position is represented in light blue/solid. The plots are complying with the expected increase of the oscillations. A second experiment is performed with different initial mechanical stiffness while all other parameters are constant. The results reported in Fig. 11.3 show the trajectory of the link depending on the mechanical stiffness. Unlike the first experiment, the oscillation are expected to be reduced when the mechanical stiffness is increased. Indeed, a stiff mechanism minimizes the error between the desired and the achieved torque since the system requires less motion for the same change of torque. Moreover, increasing the initial pretension increases the friction in the tendon guiding and leads to a higher damping ratio. It should be noted that in the high mechanical stiffness case, the initial tendon load is so high that the stick-slip effects in the joint are preventing the link to reach the desired joint position

Remarks about the singular perturbation approach In the case of the singular perturbation approach, the controller design is based on the assumption that the two controllers are independent. Several experiments confirmed that oscillations can appear when the desired joint stiffness is modified. Fig. 11.4 shows that the resonance frequency is shifted if the mechanical stiffness is modified, thus confirming that the singular perturbation approach may only be valid across a restricted frequency range.

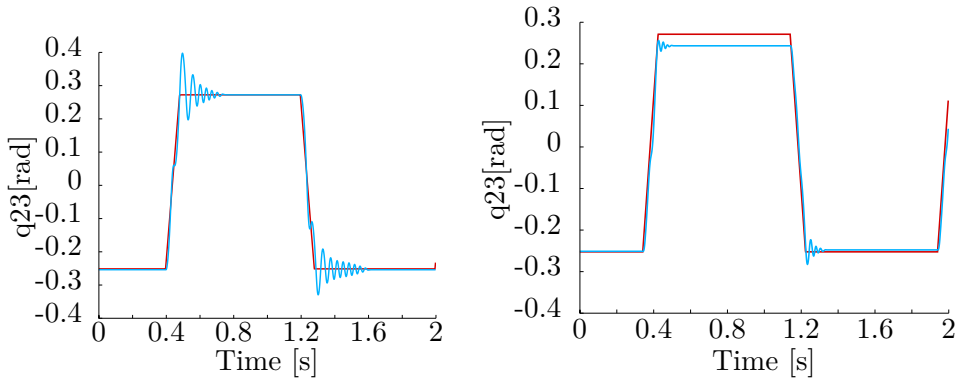

(a) Low mechanical stiffness (b) High mechanical stiffness

Figure 11.3: Experiment: step response for two different mechanical stiffness

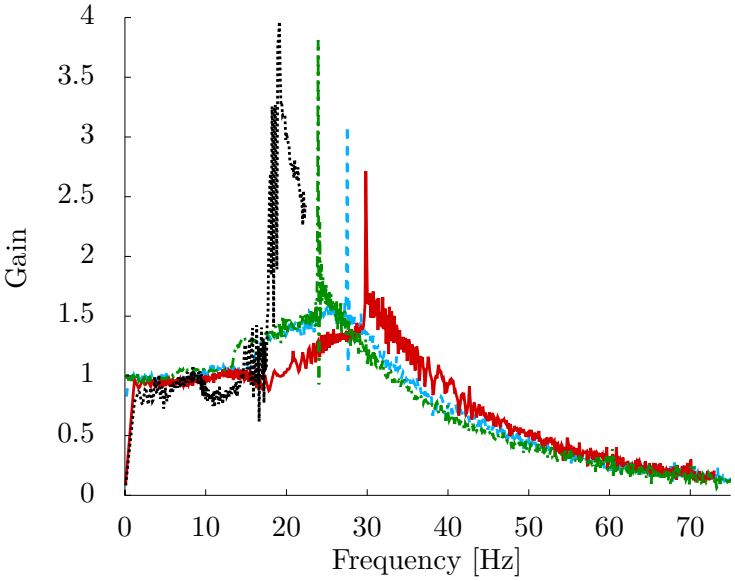

Figure 11.4: Experiments: gain diagram of the output link position across a frequency range and for different stiffness. The responses are obtained by a sinusoidal sweep input for the desired link. It can be observed that the resonance frequency is shifted when the mechanical stiffness is modified.

11.7 Discussion

This chapter presented two approaches for the control of a flexible joint: the singular perturbation approach and the cascaded approach. In both cases the stability can be established by the use of the Lyapunov stability theorems. The singular perturbation case simply neglects the influence of the force tracking error. However, it was experimentally verified that the validity of the time scale separation assumption depends on the mechanical stiffness settings. The cascaded stability analysis is more involved but explicitly includes the tendon force error, thus is independent of the mechanical stiffness. It is important to note that the tendon controller used for the proof must depend on $\boldsymbol{f}_{\mathrm{t}}$ and not on $\boldsymbol{\theta}$ in order to obtain a cascaded form. The controller was experimentally tested and demonstrated a basic performance.

12 Direct pole placement

The singular perturbation method is restricted to the domains where the two subsystems, that is the link side impedance controller and the tendon force controller, do not interact. The cascaded method does not require such a restriction at the cost of a more complex choice of the gains. In order to improve the controller, in the sense that the time scale hypothesis is not required anymore, it is necessary to use a more global approach. The concept of direct pole placement using a feedback controller is, historically, one of the first methods applied to control multi-DOF systems. It is described by a slightly different form in nearly all control books, for example in [131, p. 176]. The method consists in computing the closed-loop poles of the system and designing the feedback such that the poles are placed as desired. The very notion of poles being restricted to linear system (there exist some extensions work for nonlinear systems, e. g. [132] for an introduction or [133] for an application to discrete systems). The proposed approaches in the literature are mostly focusing on two aspects: whether the closed-loop system reaches the targeted behavior (locally) and, since the controllers are by construction locally stable, how large is the actual region of stability and how to enlarge it.

This chapter focuses on the placement of the poles of the system and the sensitivity of the poles around the nominal model. One important question is how sensitive is the controller w. r. t. the plant modeling errors. A more practical question is the choice of the poles. Indeed, whereas selecting a negative real part for the poles is trivially ensuring stability, it is challenging to *imagine* which poles should be used for a fourth order system that will result in a *good* behavior.

The chapter is organized as follows. First, a simple example is proposed to illustrate the method. It is shown that the identification of the closed-loop poles to the poles of a well-known system is an intuitive method. Then, the method is applied to a linear flexible joint model which is a fourth order system. The closed-loop solutions are given and, by identification, the poles are placed. Finally, a robustness analysis is proposed. The sensitivity of the poles w. r. t. the modeling errors is studied. To this end, modeling errors are introduced and the poles of the system under the nominal controller are calculated. It is shown that the method is highly sensitive to the system stiffness. Since the method is not robust to modeling errors, even in the linear case, the method is not applied to the nonlinear case. However, the nonlinear case is handled in a later chapter with the help of the state dependent Riccati equations.

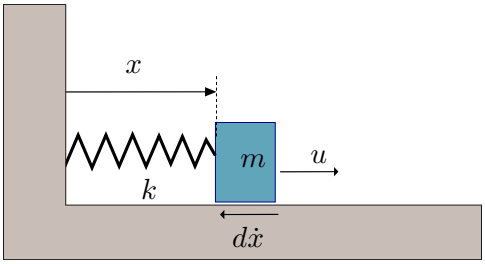

Figure 12.1: Simple mass spring damper system. The viscous friction generated by the ground is denoted $d\dot{x}$.

12.1 Introductory example

This section is an introduction example to the pole placement method. The reader familiar with linear control theory can safely skip this section. The equation of a simple spring-mass-damper system (cf. Fig. 12.1) is

$$m\ddot{x} = -d\dot{x} - kx + u \ , \tag{12.1}$$

where $m \in \mathbb{R}$ is the mass of the solid, $(x, \dot{x}) \in \mathbb{R}^2$ are the position and velocity of the mass, $(k, d) \in \mathbb{R}^2$ are spring constant and damping coefficient. The system input is denoted $u \in \mathbb{R}$. Assuming that the complete state is available (at least through some observer), the controller equation can take the general form of a static (i. e. the coefficient are constant w. r. t. time) state feedback

$$u = -\beta\dot{x} - \alpha x \ , \tag{12.2}$$

where $(\alpha, \beta) \in \mathbb{R}^2$ are time invariant gains. Under the action of the controller the normalized closed-loop equation is

$$\ddot{x} + \frac{(d+\beta)}{m}\dot{x} + \frac{(k+\alpha)}{m}x = 0 \ . \tag{12.3}$$

Equation (12.3) is nothing else than a linear, second order differential equation in x with constant coefficients. Trivially, the solutions of this second order equation are

$$\begin{array}{l} \gamma_1 = \frac{-(d+\beta)-\sqrt{(d+\beta)^2-4m(k+\alpha)}}{2m} \\ \gamma_2 = \frac{-(d+\beta)+\sqrt{(d+\beta)^2-4m(k+\alpha)}}{2m} \end{array} \ . \tag{12.4}$$

Transformed into the time domain, the solution is,

$$x(t) = Ae^{-\gamma_1 t} + Be^{-\gamma_2 t}, t > 0, \tag{12.5}$$

where $(A, B) \in \mathbb{R}^2$ are constants depending on the initial conditions. The solution might oscillate or not and converge or not, depending on whether

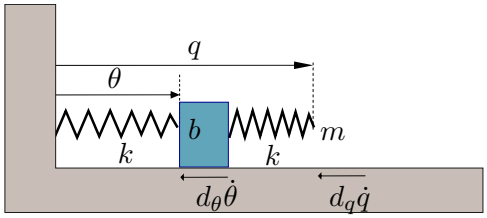

Figure 12.2: Double spring mass damper system in the case of a flexible joint model

γ_1, γ_2 are complex or not and whether their real part is positive or negative. Therefore, directly selecting the poles γ_1, γ_2 such that they have a negative real part ensures stability. However, it does not allow an easy design of the system behavior since the combination of the contributions of the poles is not intuitive. It is easier to identify the system to a well-known system, such as a harmonic oscillator, and select the parameters accordingly. Identifying the coefficients of the normalized equation to the coefficients of a damped harmonic oscillator gives the following equation to be solved:

$$\ddot{x} + \frac{(d+\beta)}{m}\dot{x} + \frac{(k+\alpha)}{m}x = \ddot{x} + 2\xi\omega_0\dot{x} + \omega_0^2 x \ , \tag{12.6}$$

where $\omega_0 \in \mathbb{R}$ and $\xi \in \mathbb{R}$ are the undamped angular frequency and the damping ratio of the harmonic oscillator. For a given choice of ω_0 and ξ, one obtains the controller gains $(\alpha, \beta) \in \mathbb{R}^2$ that result in the desired behavior. The gains are given by

$$\begin{array}{rcl} \alpha & = & m\omega_0^2 - k \\ \beta & = & 2m\xi\omega_0 - d \end{array} . \tag{12.7}$$

The method is simple and can be applied to many linear systems. It is important to note that, although the method does not enforce it, selecting poles that are far from the natural behavior might practically lead to instabilities.[1]

12.2 Fourth order model

The most simple model for a flexible joint system is a fourth order system. Therefore, in this section, the pole placement method is applied on the joint model depicted in Fig. 12.2. Referring to the modeling of Chapter 5, the joint equations are given by

$$\begin{array}{rcl} m\ddot{q} & = & -d_{\mathrm{q}}\dot{q} + k(\theta - q) \\ b\ddot{\theta} & = & -d_\theta\dot{\theta} - k(\theta - q) + u \end{array} , \tag{12.8}$$

[1] unmodeled dynamics or actuator saturation invalidate the stability proof.

where $(m, b) \in \mathbb{R}^2$ are the masses, $(q, \dot{q}, \theta, \dot{\theta}) \in \mathbb{R}^4$ are the link position, the link velocity, the motor position and the motor velocity. The damping coefficients and the spring constant are represented by $(d_\mathrm{q}, d_\theta, k) \in \mathbb{R}^3$. The actuator torque is represented by $u \in \mathbb{R}$. Defining the state vector $\boldsymbol{x} = [q, \dot{q}, \theta, \dot{\theta}]^T$, the dynamics can be written in matrix form

$$\dot{\boldsymbol{x}} = \boldsymbol{A}\boldsymbol{x} + \boldsymbol{K}\boldsymbol{B}u, \tag{12.9}$$

where $\boldsymbol{A} \in \mathbb{R}^{4\times4}$, $\boldsymbol{B} \in \mathbb{R}^{4\times1}$ are called the dynamic matrix and the input matrix. $\boldsymbol{K} \in \mathbb{R}^4$ is the feedback gain vector. Following (12.8) the matrices are given by

$$\boldsymbol{A} = \begin{bmatrix} 0 & 1 & 0 & 0 \\ -\frac{k}{m} & -\frac{d_\mathrm{q}}{m} & \frac{k}{m} & 0 \\ 0 & 0 & 0 & 1 \\ \frac{k}{b} & 0 & -\frac{k}{b} & -\frac{d_\theta}{b} \end{bmatrix} \tag{12.10}$$

and

$$\boldsymbol{K} = \begin{bmatrix} \alpha_1 & \alpha_2 & \alpha_3 & \alpha_4 \end{bmatrix}^T . \tag{12.11}$$

With the help of a symbolic calculation software, the coefficients of the characteristic polynomial of the closed-loop system are

$$\begin{bmatrix} -\frac{k}{mb}(\alpha_1 + \alpha_3) \\ \frac{-d_\mathrm{q}\alpha_3 - k(\alpha_2 + \alpha_4 - d_\mathrm{q} - d_\theta)}{mb} \quad \frac{d_\mathrm{q}d_\theta - m\alpha_3 + k(m+b) - d_\mathrm{q}\alpha_4}{mb} \\ \frac{md_\theta - m\alpha_4 + d_\mathrm{q}b}{mb} \\ 1 \end{bmatrix} . \tag{12.12}$$

To guarantee exponential stability it is necessary that the roots of the polynomial have negative real parts. However, it is neither easy to select the gains $\boldsymbol{\alpha}$ nor intuitive to choose the amplitude of the real part. Indeed, it is important to remember that although the theory guarantees exponential stability, it is practically impossible to use arbitrarily large gains. Similar to the case of the mass spring damper, if the coefficients of a well-known fourth order system are available it is possible to proceed by identification. Motivated by the mechanical structure of the system, one choice consists in taking the dynamics of a double harmonic oscillators as a target.

$$(s^2 + 2s\xi_1\omega_1 + \omega_1^2)(s^2 + 2s\xi_2\omega_2 + \omega_2^2) = 0 \ , \tag{12.13}$$

where s is the Laplace transform of x and $(\xi_1, \xi_2, \omega_1, \omega_2) \in \mathbb{R}^4$ are the damping ratios and the undamped angular frequencies of the harmonic oscillators.

By identification of the coefficients, one obtains a set of equations

$$\begin{array}{c} -\dfrac{k}{mb}(\alpha_1+\alpha_3)=\omega_1^2\omega_2^2 \\ \dfrac{-d_{\mathrm{q}}\alpha_3-k(\alpha_2+\alpha_4-d_{\mathrm{q}}-d_\theta)}{mb}=2(\xi_2\omega_1^2\omega_2+\xi_2\omega_1\omega_2^2) \\ \dfrac{d_{\mathrm{q}}d_\theta-m\alpha_3+k(m+b)-d_{\mathrm{q}}\alpha_4}{mb}=\omega_1^2+4\xi_1\xi_2\omega_1\omega_2+\omega_2^2 \\ \dfrac{md_\theta-m\alpha_4+d_{\mathrm{q}}b}{mb}=2(\xi_1\omega_1+\xi_2\omega_2) \end{array}, \tag{12.14}$$

where the unknowns are $(\alpha_1, \alpha_2, \alpha_3, \alpha_4) \in \mathbb{R}^4$. The system of equations can be written as

$$\boldsymbol{J}\boldsymbol{\gamma} = \boldsymbol{\mu}, \tag{12.15}$$

where $\boldsymbol{\gamma} = [\alpha_1, \alpha_2, \alpha_3, \alpha_4]^T$ is the vector of unknowns, $\boldsymbol{\mu} \in \mathbb{R}^4$ is the vector of desired values and $\boldsymbol{J}$ is the Jacobian matrix given by,

$$\boldsymbol{J} = \frac{k}{bm}\begin{bmatrix} -1 & 0 & -1 & 0 \\ 0 & -1 & -\frac{d_{\mathrm{q}}}{k} & -1 \\ 0 & 0 & -\frac{m}{k} & -\frac{d_{\mathrm{q}}}{k} \\ 0 & 0 & 0 & -\frac{m}{k} \end{bmatrix}. \tag{12.16}$$

The system has solutions as long as $\boldsymbol{J}$ is invertible, that is if the determinant is not 0. The determinant of $\boldsymbol{J}$ is $\det(()\boldsymbol{J}) = \frac{k^2}{m^2b^4} > 0$. Therefore, a unique solution for the selection of the gains always exists.

12.3 Robustness analysis

The controller gains obtained in the last section are, by construction, leading to a system whose characteristic equation is given by (12.13) Using the numerical values reported in Table 12.1, the associated poles are

$$\begin{array}{c} -100+0.66i \\ -100-0.66i \\ -10+0.38i \\ -10-0.38i \end{array} \tag{12.17}$$

showing that the nominal system under the pole placement controller is exponentially stable. The corresponding gains for the state feedback are (numerical values from Table 12.1)

$$\begin{array}{c} \alpha_1 = 4395 \\ \alpha_2 = 6.177 \\ \alpha_3 = -4395 \\ \alpha_4 = 288.99 \end{array} \tag{12.18}$$

Table 12.1: Numerical values used to evaluate the poles

Symbol	Value	Units
b	$2e-3$	$kg\,m^2$
m	$4e-7$	$kg\,m^2$
k	0.605	Nm/rad
d_{q}	0.0012	$Nm/(rad/s)$
d_θ	0.0012	$Nm/(rad/s)$
ω_1	100	rad/s
ω_2	30	rad/s
ξ_1	0.7	
ξ_2	0.7	

It is interesting to note that the damping coefficient for the link is positive. It implies that the controller is trying to reduce the link friction by *pushing* the link. Although the closed-loop system is stable, this type of feedback is not recommended in practice. As with all model-based designs, the exact plant parameters are not perfectly known and it is important to study the influence of the plant model errors on the overall stability. Modifying the real plant parameters from $k = 0.605Nm/rad$ to $k = 0.600Nm/rad$ and recomputing the poles yields

$$\begin{matrix} -318.78 \\ 53.27 + 225.14i \\ 53.27 - 225.14i \\ -0.058 \end{matrix} \tag{12.19}$$

The modified plant under the nominal pole placement controller has a positive real part leading to an unstable system. It indicates that the pole placement method is very sensitive to the plant modeling errors, at least around the selected target dynamics. A more accurate sensitivity analysis is obtained by a parametric analysis. All quantities are fixed (to the nominal parameters of Table 12.1) but one that is varied across an uncertainty range. The root locus plots are then used to evaluate the sensitivity to each parameter. Fig. 12.3 depicts the sensitivity of open loop the poles w. r. t. to the spring stiffness and the link damping. Fig. 12.4 depict the sensitivity of the closed-loop poles w. r. t. to the link stiffness. It can be seen that the poles of the closed-loop plant are very sensitive to the link stiffness. The range of stiffness that is tested is a realistic range of adjustability of the stiffness. The simulation highlights the limited robustness of the controller, even though this particular choice of feedback gains does not lead to an unstable system.

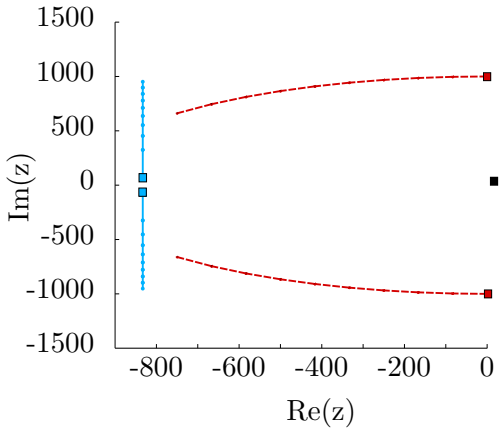

Figure 12.3: Open loop poles depending on the stiffness and the link damping. The influence of the link stiffness $K = [0.43, 1.15]$ is depicted in light blue/solid. The influence of the link damping $D_\mathrm{q} = [0.43, 1.15]$ is depicted in red/dashed. In both cases the square indicates the start values. The third and fourth poles are depicted in black and do not change significantly.

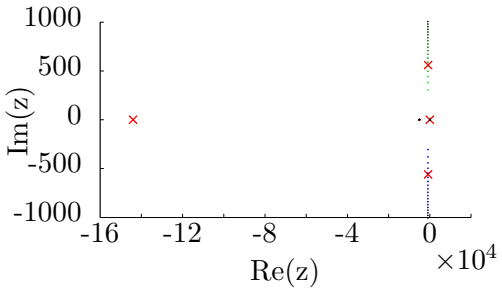

Figure 12.4: Closed-loop poles depending on the stiffness $K = [0.43, 1.15]$. The nominal poles are indicated by squares. It can be seen that the poles are sensitive to the link stiffness.

12.4 Discussion

As highlighted in the previous section, the robustness of the method is very limited for the selected target dynamics. Because of the sensitivity, it is not guaranteed that the overall system will be robust enough to cope with the modeling errors unless a very conservative performance is selected. Indeed, despite the extensive modeling, the stiffness of the Awiwi Hand is not precisely known. Moreover, the method is only local thus the stiffness change around the nominal position is only treated as a disturbance. The modeling errors, the calibration errors, the unmodeled dynamics, and the linearization approximations would practically lead to a marginally stable system. One major concern is that, if the target dynamics is far from the natural behavior, the magnitude of the control input might be extremely large. If the controller action is too large, the nonlinearities associated with the actuator saturation might introduce, as well, instabilities. Therefore, the idea of using a full state feedback controller around each linearization point, as reported in [77] is not applied. Their approach is successful mainly because the range of stiffness they considered is higher and their link inertia much larger. As a result their system is less sensitive to the modeling errors.

13 Optimal control

The direct pole assignment method did not account for the magnitude of the control input, resulting in an unpractical command law. Although theoretically very capable, its robustness revealed to be practically limited for the selected choice of target dynamics. In this chapter the focus lies on finding a method that mitigates the costs of the error and the magnitude of the input, thus implicitly selects good target dynamics. A possible way to express the objective mathematically is to formulate an optimization problem in the form

$$\min_{u(t)} \int_0^t (\boldsymbol{x}(t)^T \boldsymbol{Q} \boldsymbol{x}(t) + u(t)^T R u(t)) dt \ , \tag{13.1}$$

where $\boldsymbol{x}(t) \in \mathbb{R}^2$ and $u(t) \in \mathbb{R}$ are the state vector and the input vector. $\boldsymbol{Q} \in \mathbb{R}^{2\times 2}$ and $R \in \mathbb{R}$ are a positive definite matrix and a scalar that represent sthe cost of the error and the cost of the input. In this chapter, a linear quadratic regulator (LQR) is analyzed. It serves as an introduction to the SDRE method presented in the next chapter. The chapter is organized as follows. First, a simple example is proposed to illustrate the method. In the second section, the method is applied to the linear flexible joint model, which is a Linear Time Invariant system (LTI). Finally, simulations are performed to evaluate the results.

13.1 Introduction example

Similar to the previous chapters, a single spring mass damper is used to introduce the method. The equation of a simple single spring mass system (Fig. 13.1) is

$$m\ddot{x} = -d\dot{x} - kx + u \ , \tag{13.2}$$

where $m \in \mathbb{R}$ is the mass of the solid, $(x, \dot{x}) \in \mathbb{R}^2$ are the mass position and velocity, and $(k, d) \in \mathbb{R}^2$ are some positive spring constant and damping coefficients. The system input, an external force, is denoted $u \in \mathbb{R}$. The

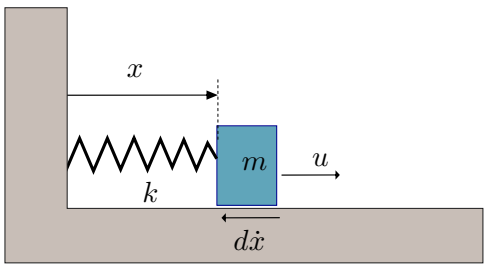

Figure 13.1: Single mass-spring-damper.

regulator feedback has the form

$$u(t) = -\boldsymbol{K}(t)^T \boldsymbol{x}(t) \ , \tag{13.3}$$

where $\boldsymbol{x}(t) \in \mathbb{R}^2$ is the state vector and $\boldsymbol{K}(t) = R^{-1}\boldsymbol{B}^T\boldsymbol{S}(t)$ is the vector of the state feedback gains. $\boldsymbol{S}(t)$ is the solution of the differential Riccati equation

$$\frac{d\boldsymbol{S}(t)}{dt} = -\boldsymbol{S}(t)\boldsymbol{A} - \boldsymbol{A}^T\boldsymbol{S}(t) + \boldsymbol{S}(t)\boldsymbol{B}R^{-1}\boldsymbol{B}^T\boldsymbol{S}(t) - \boldsymbol{Q} \ , \tag{13.4}$$

where $\boldsymbol{A} \in \mathbb{R}^{2\times 2}$ denotes the dynamic matrix. For an infinite time horizon, the equation is the algebraic Riccati equation (ARE) given by

$$\boldsymbol{S}\boldsymbol{A} + \boldsymbol{A}^T\boldsymbol{S} - \boldsymbol{S}\boldsymbol{B}R^{-1}\boldsymbol{B}^T\boldsymbol{S} + \boldsymbol{Q} = 0 \ . \tag{13.5}$$

In such a case, all matrices are constant and solving the ARE given by (13.5) for $\boldsymbol{S}$ yields the optimal linear regulator gains. Solving the ARE is not critical since it can be performed offline and several solvers are available.

13.2 Fourth order system

According to the previous chapter, a double mass spring damper system is described by

$$\dot{\boldsymbol{X}} = \boldsymbol{A}\boldsymbol{X} + \boldsymbol{B}u \ , \tag{13.6}$$

where the state matrix $\boldsymbol{A} \in \mathbb{R}^{4\times 4}$ and the input matrix $\boldsymbol{B} \in \mathbb{R}^{4\times 1}$ are given by

$$\boldsymbol{A} = \begin{bmatrix} 0 & 1 & 0 & 0 \\ -\frac{k}{m} & -\frac{d_q}{m} & \frac{k}{m} & 0 \\ 0 & 0 & 0 & 1 \\ \frac{k}{b} & 0 & -\frac{k}{b} & -\frac{d_\theta}{b} \end{bmatrix} \tag{13.7}$$

and

$$\boldsymbol{B} = \begin{bmatrix} 0 \\ 0 \\ 0 \\ 1/b \end{bmatrix} \ . \tag{13.8}$$

The optimal feedback gains are obtained by solving the ARE equation. Defining the state cost matrix $\boldsymbol{Q} \in \mathbb{R}^{4\times 4}$ and the input cost $R \in \mathbb{R}$ by

$$\boldsymbol{Q} = \begin{bmatrix} 10 & 0 & 0 & 0 \\ 0 & 0.01 & 0 & 0 \\ 0 & 0 & 1 & 0 \\ 0 & 0 & 0 & 0.01 \end{bmatrix} \ , \tag{13.9}$$

and

$$R = 0.01 \ , \tag{13.10}$$

Table 13.1: Parameters used for the simulation of the optimal state feedback

Symbol	Value	Units
B	$2e-3$	$kg.m^2$
M	$4e-7$	$kg.m^2$
k	0.605	Nm/rad
Q	$\begin{bmatrix} 10 & 0 & 0 & 0 \\ 0 & 0.01 & 0 & 0 \\ 0 & 0 & 1 & 0 \\ 0 & 0 & 0 & 0.01 \end{bmatrix}$	
R	$\in [0.0001, 0.01, 1]$	

MATLAB® gives the following solution

$$u = -\left[-126.21, -0.11, 159.37, 1.52\right]^T \boldsymbol{x} \ . \tag{13.11}$$

.

13.3 Simulation

The simulations are performed using the numerical solver from MATLAB®, with the parameters of Table 13.1. The link and motor positions obtained for different input costs are reported in Figure 13.2. The corresponding inputs are reported in Figure 13.3. As desired, the amplitude of the input command can be controlled by the cost matrices R and $\boldsymbol{Q}$. It should be noted that the simulations are performed with costs matrices that are not directly suitable for the real implementation. In practice, the gain matrices must be selected according to the expected performance, the noise of the sensors and the computation delays.

13.4 Discussion

The optimal control method has been applied to a linear fourth order system. In the case of such a system, the optimality problem can be reduced to the problem of solving the ARE. The method allows to specify the relative cost of the input amplitude w. r. t. the state errors. Therefore, it is possible to moderate the controller action by setting a high cost on the input. However, a limited command also results in a degraded feedback effect in terms of settling time. The plant under such a controller is guaranteed to be exponentially stable by construction. However, the method is not suitable for nonlinear plants since the problems must be written in a linear form. Moreover, solving directly the corresponding nonlinear, optimal control problem online is practically intractable.

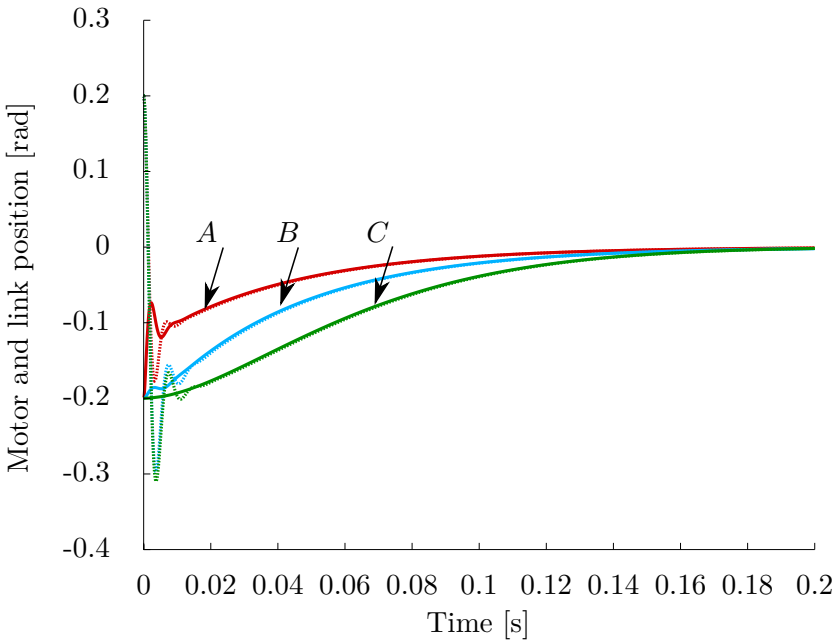

Figure 13.2: Simulation: link and motor trajectories of the plant under an optimal state feedback controller. The simulations performed with $R = 0.0001$ (resp. 0.01 and 1 are denoted by A/red (resp. B/light blue, C/green). The solid line represents the motor position whereas the dotted line represents the link position.

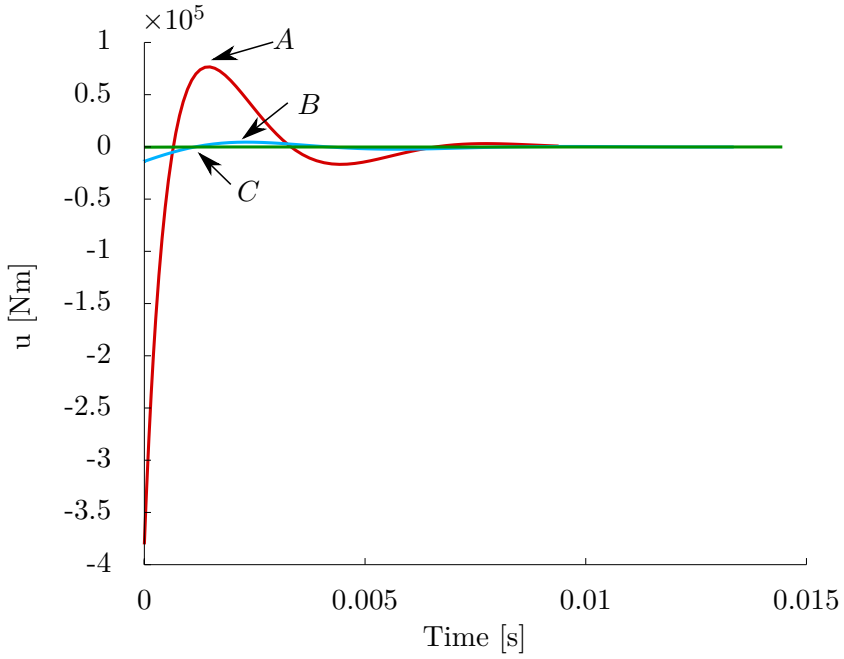

Figure 13.3: Simulation: input command of the plant under an optimal state feedback controller. The curves A/red (resp. B/light blue, C/green) are corresponding to the simulations of Figure 13.2.